Risk Behavior, Backward Bifurcation, and Vaccine Effectiveness in Disease Dynamics

Irasema Pedroza-Meza[1*], M. Adrian Acuña-Zegarra[1] and Jorge X. Velasco-Hernández[2]

[1]Departamento de Matemáticas, Universidad de Sonora, Blvd. Luis Encinas y Rosales S/N, Hermosillo, 83000, Sonora, México.
[2]Instituto de Matemáticas, UNAM-Juriquilla, Blvd. Juriquilla No. 3001, Juriquilla, 76230, Queretaro, Mexico.

*Corresponding author(s). E-mail(s): irasema.pedroza.meza@gmail.com;
Contributing authors: adrian.acuna@unison.mx jx.velasco@im.unam.mx

Abstract

Many studies have shown that vaccines are not completely effective, meaning that a vaccinated population includes both people who develop immunity from the vaccine and those who, despite being vaccinated, do not. This can be problematic, as some vaccinated individuals may mistakenly believe they are fully protected and cannot acquire the disease. This perception can significantly influence behavior, leading some vaccinated people to be less diligent in following preventive or mitigation measures.

Motivated by the above, we examine how behavioral changes in vaccinated people who do not develop immunity influence the dynamics of a directly transmitted disease and key indices such as the basic reproductive number and vaccine effectiveness. We propose a model that considers a vaccine with three facets of failure: "take", "degree", and "duration". Additionally, the behavioral change of non-immune vaccinated individuals is modeled through a parameter that adjusts their contact rate based on compliance with mitigation measures.

Our results allow us to visualize the role of behavioral change in various factors influencing disease transmission dynamics. First, we demonstrate the existence of a backward bifurcation common in models for not fully effective vaccines. Second, we define a behavioral index threshold, which serves as a key indicator for determining whether the disease persists due to behavioral effects. Finally, our results highlight that both the behavioral index and the initial value of the infected

population can play a decisive role in determining whether vaccine effectiveness reaches negative values.

Keywords: Mathematical model, Vaccine failure, Behavioral change, Vaccine efficacy, Kermack-McKendrick

1 Introduction

Motivated by the absence of complete immunity of vaccines over respiratory diseases and behavioral change induced by the action of non-pharmaceutical interventions (Seale et al., 2020), in this study we explore the impact of non-immune vaccinated individuals' behavior on disease transmission dynamics. For that aim, we formulate an extension of classic epidemiological models (Saldaña and Velasco-Hernández, 2022), incorporating vaccination, and following McLean and Blower (1993), we assume that the vaccine may present three facets of vaccine failure: "take", "degree", and "duration". We model these failures by (i) splitting the vaccinated population into two classes (immune vaccinated and non-immune vaccinated), (ii) incorporating a reduction in the transmission contact rate for the non-immune vaccinated population, and (iii) assuming that immune vaccinated individuals become fully susceptible after a certain period of time. In addition, we explore whether the proposed model presents similar phenomena to those observed in classical models that include vaccination such as backward bifurcation.

Given that vaccine-induced immunity is not complete, it becomes crucial to assess how vaccination, combined with individual behavioral responses, influences epidemic outcomes. In particular, understanding the interplay between vaccine efficacy and behavioral changes can provide insight into the effectiveness of control and mitigation strategies. The effects and efficiency of control and mitigation strategies are one of the central interests in the study of the spread of epidemics (Hsieh and Velasco-Hernandez, 1995; Hsieh, 2010; Gemmetto et al., 2014; Acuña-Zegarra et al., 2020;

Xue et al., 2021). Vaccines are a fundamental tool for the control and eradication of infectious diseases. However, the beneficial effects of the vaccine on a population can be diminished by behaviors that increase the contact rate. Vaccine efficacy is a measure of how well a vaccine protects against infection, hospitalization, and death (World Health Organization, 2021). Vaccine efficacies are not full; there is always a certain percentage of vaccinated individuals for whom the vaccine does not confer protection or the protection is weaker than the expected average (Smith et al., 1984; Halloran et al., 1991, 1992). Risk-averse and risk-prone behaviors play a significant role in the outcome of the effectiveness of a vaccine. Risk-averse behaviors reduce the contact rate, strengthening the vaccine's efficacy; on the contrary, risk-prone behaviors may increase the per capita contact rate, thus increasing the average transmissibility of the pathogen. When the last occurs, vaccinated individuals, who have weak protection, increase the susceptible pool of individuals available for disease infection, which may lead, at the population level, to the existence of multiple endemic equilibria (e.g., Kribs-Zaleta and Velasco-Hernández, 2000; Allen and van den Driessche, 2006; Kar and Mondal, 2012; Hu et al., 2012).

On the other hand, studying the consequences of different vaccine properties, particularly efficacy, on the dynamics of an epidemic outbreak is closely associated with the conditions under which oscillatory dynamics or multiple equilibrium points occur in epidemiological differential equation systems (see e.g., Kribs-Zaleta and Velasco-Hernández, 2000; Kribs-Zaleta and Martcheva, 2002; Velasco-Hernández et al., 2015). Usually, multiple endemic equilibria, resulting from a transcritical backward bifurcation, appear when the basic reproduction number is below 1 (Hadeler and Castillo-Chávez, 1995; Dushoff et al., 1998; Kribs-Zaleta and Velasco-Hernández, 2000; Greenhalgh et al., 2001; Arino et al., 2004). Therefore, one of our objectives in this work is to study the role of vaccination and behavioral change in generating this atypical subthreshold phenomenon.

Many mathematical models assume that imperfect immunization reduces the effective contact rate (see e.g., Gumel, 2012; Safan and Rihan, 2014; Saldaña and Velasco-Hernández, 2021; Acuña-Zegarra et al., 2021). From the modeling point of view, we characterize a vaccine with three essential parameters. One of them is coverage, the percentage of the population vaccinated; the second is immunity, which is the period that it takes a vaccinated individual on which the vaccine works effectively to lose the immunity that the vaccine confers. The third is the vaccine efficacy, which is the percentage of the vaccinated population that is genuinely protected (World Health Organization, 2021). In the recent COVID-19 pandemic, several vaccines have reached above 90% efficacies (Colmegna et al., 2023; Wu et al., 2024) while others have reached between 70% and 80% (Ghiasi et al., 2021; Sadoff et al., 2022). For other infectious diseases, these efficacies may vary widely (Diaz Granados et al., 2014; Ray et al., 2017). We call the combination of these three parameters—coverage, efficacy, and waning time—as the vaccination policy, with the occurrence of a backward bifurcation depending on the magnitudes of each parameter (Arino et al., 2003).

In what follows, we present and analyze a mathematical model that incorporates behavioral change and vaccine failures. We formulate our mathematical model in Section 2. Section 3 presents the qualitative analysis which include the existence of backward bifurcation. Section 4 shows numerical simulations exploring the impact of some parameters on disease transmission dynamics and some indexes. Finally, we present our conclusions in Section 5.

2 Mathematical model

The classic models incorporating vaccination assume that all susceptible individuals are vaccinated at a specific rate and that the vaccine's efficacy is reflected in the reduction of the contact rate: the higher the efficacy of the vaccine, the smaller the percentage reduction of the contact rate (Kribs-Zaleta and Velasco-Hernández, 2000;

Arino et al., 2003; Safan and Rihan, 2014). This usual assumption may lead to a backward bifurcation. The backward bifurcation is a transcritical bifurcation where the branch of endemic equilibria arises with a negative slope, triggering the possibility of multiple endemic states below the threshold value of the reproductive number. In this case, we will have two locally asymptotically stable states and one unstable equilibrium point.

One of the simplest models that addresses this situation is based on that proposed by Kribs-Zaleta and Velasco-Hernández (2000)

$$\begin{aligned}
\dot{S} =& \mu N - \beta \frac{SI}{N} - (\mu + \phi)S + \omega V + \xi R \\
\dot{V} =& \phi S - (1-\sigma)\beta \frac{VI}{N} - (\omega + \mu)V \\
\dot{I} =& \beta \frac{SI}{N} + (1-\sigma)\beta \frac{VI}{N} - (\mu + \gamma)I \\
\dot{R} =& \gamma I - (\mu + \xi)R,
\end{aligned} \tag{1}$$

where S, V, I, and R denote the susceptible, vaccinated, infectious, and recovered compartments, respectively; μ, β, ϕ, ω, γ, and ξ represent the mortality, effective contact, vaccination, vaccine waning, recovery, and natural immunity waning rates, respectively. Here, σ denotes the vaccine efficacy, thus allowing the interpretation of $1-\sigma$ as the net reduction in the magnitude of the contact rate. In Model (1), we represent vaccine coverage as a rate (number of individuals vaccinated per unit of time), and, as already mentioned above, the effect of vaccine efficacy is represented in the term $(1-\sigma)\beta$ in the second equation. The interpretation is that efficacy reduces the contact rate; the higher the efficacy, the lower the effective contact rate. This produces the typical behavior of epidemic models: if the reproduction number is above one, a transcritical bifurcation occurs, a branch of locally asymptotically stable endemic equilibria arises, and the disease-free equilibrium becomes unstable. However, a backward bifurcation appears in specific ranges of (ϕ, ω, σ) (Kribs-Zaleta and Velasco-Hernández, 2000).

Model (1) considers vaccination as a tool to reduce the contact rate. Similarly, behavioral changes caused by measures of non-pharmaceutical interventions have an analogous effect.

This study extends the classic model involving vaccination, to separate the effects of behavioral change and vaccination on reducing the effective contact rate. Our Model considers an imperfect vaccine with three possible types of failures: failure in degree (as a leaky vaccine), failure in duration (as a waning vaccine), and failure in uptake (as an all-or-nothing vaccine) (McLean and Blower, 1993; Magpantay et al., 2014). Consequently, the vaccinated population has two classes: those who acquire immunity from the vaccine, referred to as *immune vaccinated* (V_+), and those that acquire weak immunity or not at all, which from now on will be referred to as *non-immune vaccinated* (V_-). By assumption, immune-vaccinated individuals are fully protected from infection during the period during which the vaccine is effective. On the other hand, due to the vaccine's degree of failure, non-immune vaccinated individuals can still become infected, albeit at a different rate than susceptible individuals (S). Moreover, we assume that individuals who receive the vaccine may not adhere to prevention and mitigation directives for the disease. As detailed below, we model this possibility as varying transmission rates for V_- population through a behavioral index ψ. Figure 1 illustrates the proposed model.

The vaccination rate (ϕ) is determined by the flow of susceptible individuals to the vaccinated classes. However, coverage is the common parameter for determining a vaccination policy. Motivated by the above, this rate now can be modulated through the percentage coverage denoted by p (Acuña-Zegarra et al., 2021).

$$\phi = -\frac{\ln(1-p)}{T} \ ,$$

where T is the time over which vaccine coverage is achieved.

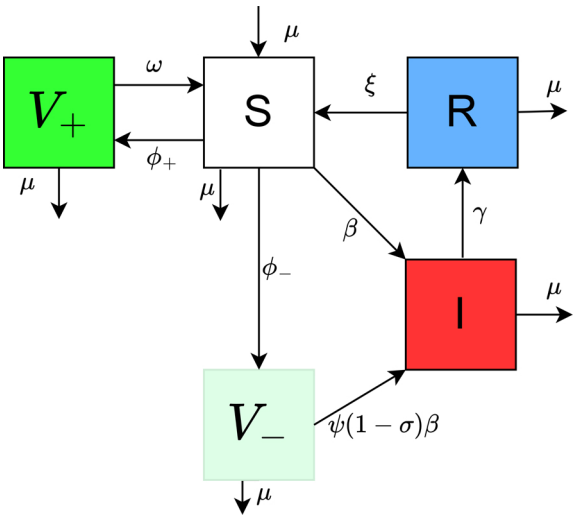

Fig. 1: Diagram for Model (3) where susceptible, immune vaccinated, non-immune vaccinated, infected and recover, are represented by S, V_+, V_-, I and R respectively. Table 1 contains the definition of parameters.

In this study, we propose to split the vaccination rate into two rates, such that their sum produces the original vaccination rate (ϕ). Following a similar process to obtain ϕ, we now define $p\sigma$ as the effective vaccinated proportion, or effective coverage, where σ represents the vaccine efficacy. Thus, the effective vaccination rate is given by

$$\phi_+(\sigma) = -\frac{\ln(1-p\sigma)}{T},$$

Finally, since $\phi = \phi_+(\sigma) + \phi_-(\sigma)$, we can define $\phi_-(\sigma)$ as the vaccination failure rate and its expression is given by,

$$\phi_-(\sigma) = \frac{1}{T}\ln\left(\frac{1-p\sigma}{1-p}\right) .$$

Note that $\phi_+(\sigma)$ and $\phi_-(\sigma)$ are well-defined for any $T > 0$ and can be adjusted via the coverage $p \in [0, 1)$. Moreover, if vaccine efficacy is null ($\sigma = 0$), then no one acquires immunity ($\phi_- = \phi$ and $\phi_+ = 0$). Conversely, if vaccine efficacy is full ($\sigma = 1$), then all vaccinated individuals acquire immunity ($\phi_+ = \phi$ and $\phi_- = 0$).

2.1 Model equations

Using the above definitions, we present our mathematical model:

$$
\begin{aligned}
\dot{S} = &\quad \mu N - \beta \tfrac{SI}{N} - (\mu + \phi)S + \omega V_+ + \xi R \\
\dot{V}_+ = &\ \phi_+(\sigma)S - (\mu + \omega)V_+ \\
\dot{V}_- = &\ \phi_-(\sigma)S - \psi(1-\sigma)\beta \tfrac{V_- I}{N} - \mu V_- \\
\dot{I} = &\quad \beta \tfrac{SI}{N} + \psi(1-\sigma)\beta \tfrac{V_- I}{N} - (\mu + \gamma)I \\
\dot{R} = &\quad \gamma I - (\mu + \xi)R
\end{aligned}
\tag{2}
$$

where N is the total population size, i.e. $N = S + V_+ + V_- + I + R$ which is constant. Table 1 presents a summary of our parameter definitions. Observe that the immune vaccinated individuals V_+ have temporary immunity and return to the susceptible compartment after $1/\omega$ units of time. Also, the immune vaccinated individuals (V_+) get their immunity through the effective vaccination rate (ϕ_+), while the non-immune but vaccinated individuals (V_-) receive the vaccine but are either partially or not immunized. This occurs at a rate (ϕ_-). The non-immune vaccinated individuals (V_-) can be infected, depending on the vaccine efficacy (σ), which affects not only the coverage rate, as described above, but also reduces the effective contact rate by a proportion $1 - \sigma$; ψ represents the possible reduction of the effective contact rate due to behavioral acts, even when an individual is not effectively vaccinated: behavior may induce a decrease in the effective contact rate beyond that induced by the vaccine i.e.,the effective contact rate can be reduced due to the vaccine (efficacy) and behavioral or non-pharmaceutical actions. The I equation receives those individuals from S and V_- classes. Finally, we assume that the disease generates natural temporary immunity, so after $1/\xi$ units of time, these individuals return to the susceptible pool.

Table 1: Parameter definitions for Model (2).

Parameter	Description
β	effective contact rate
μ	natural death rate
γ	recovery rate
$1/\omega$	waning time
$1/\xi$	period of natural immunity
σ	vaccine efficacy
ψ	behavioral index
ϕ_-	vaccination failure rate
ϕ_+	effective vaccination rate

To simplify the analysis, we rescale the total population so that $N = 1$ and Model (2) is reduced to four equations. Thus, our mathematical model becomes:

$$\begin{aligned}
\dot{V}_+ &= \phi_+(\sigma)(1 - V_+ - V_- - I - R) - (\mu + \omega)V_+ \\
\dot{V}_- &= \phi_-(\sigma)(1 - V_+ - V_- - I - R) - \psi(1 - \sigma)\beta I V_- - \mu V_- \\
\dot{I} &= \beta(1 - V_+ - V_- - I - R)I + \psi(1 - \sigma)\beta I V_- - (\mu + \gamma)I \\
\dot{R} &= \gamma I - (\mu + \xi)R
\end{aligned} \tag{3}$$

The following proposition holds (proof is given in Section A).

Proposition 1. *Let* $\Omega = \{(V_+, V_-, I, R) | 0 \leq V_+, 0 \leq V_-, 0 \leq I, 0 \leq R, V_+ + V_- + I + R \leq 1\}$. *Then* Ω *is a positively invariant set under the flow of Model* (3).

3 Equilibrium states

We set the equations (3) equal to zero to calculate the equilibrium points and solve for the state variables.

3.1 Disease-free equilibrium and reproduction number

The disease-free equilibrium (P_0) of Model (3) always exists. This equilibrium is obtained by assuming the absence of the disease $I = 0$, rendering:

$$P_0 = (V_{+0}, V_{-0}, I_0, R_0) = \left(V_{+0}^*, V_{-0}^*, 0, 0\right),$$

with

$$V_{+0}^* = \frac{\phi_+(\sigma)\mu}{\mu(\mu+\phi+\omega)+\phi_-(\sigma)\omega}, \quad V_{-0}^* = \frac{\phi_-(\sigma)(\mu+\omega)}{\mu(\mu+\phi+\omega)+\phi_-(\sigma)\omega}.$$

Using the method of the next generation matrix (Van den Driessche and Watmough, 2002), we calculate the basic reproductive number R_0 of Model (3). R_0 has the structure

$$R_0(\sigma) = R_S(\sigma) + R_{V_-}(\sigma) \tag{4}$$

where

$$R_S(\sigma) = \frac{\beta}{(\mu+\gamma)}\frac{\mu(\mu+\omega)}{\mu(\mu+\phi+\omega)+\phi_-(\sigma)\omega}, \; R_{V_-}(\sigma) = \frac{\beta}{(\mu+\gamma)}\frac{\psi(1-\sigma)\phi_-(\sigma)(\mu+\omega)}{\mu(\mu+\phi+\omega)+\phi_-(\sigma)\omega}$$

R_0 can be expressed as the sum of two terms: R_S is the contribution of the susceptible population to secondary infections, and R_{V_-} is the contribution of the non-immune vaccinated population. Moreover, the latter includes the impact of the change of behavior (ψ), vaccination rate (ϕ) and vaccine efficacy (σ). In Section 4.3 we will explore the impact of σ on R_0.

Proposition 2. *The disease-free equilibrium* (P_0) *is locally asymptotically stable for* $R_0 < 1$ *and unstable for* $R_0 > 1$.

The proof is standard and is omitted.

3.2 Endemic equilibria

Endemic equilibria represent a state in which a disease persists in a population over time. Equating the right side of Model (3) to zero and assuming that $I \neq 0$, the endemic equilibrium is given by the following equations:

$$V_+ = \frac{\phi_+(\psi(1-\sigma)\beta I^*] + \mu)[(\mu+\xi) - (\mu+\xi+\gamma)I^*]}{Q}, \qquad R = \frac{\gamma}{(\mu+\xi)} I^*$$

$$V_- = \frac{\phi_-(\mu+\omega)[(\mu+\xi) - (\mu+\xi+\gamma)I^*]}{Q},$$

where $Q = (\mu+\xi)[(\psi(1-\sigma)\beta I^*] + \mu)(\mu+\omega) + \phi_+(\psi(1-\sigma)\beta I + \mu) + \phi_-(\mu+\omega)]$, and I^* is given by the solution of:

$$P(I, R_0) = -AI^2 + BI + C \tag{5}$$

with

$$\begin{aligned}
A &= \frac{\mathcal{T}m}{(\mu+\xi)} R_0 \\
B &= (R_0 - D)\,\mathcal{T} \\
D &= \frac{\beta}{\mathcal{T}}((\mu+\omega)(\mu+\psi(1-\sigma)\phi_-)(1+\mu+\xi+\gamma) \\
&\quad + (\mu+\xi)(\mu+\gamma)(\mu+\omega+\phi_+)\psi(1-\sigma) - (\mu+\omega)(\mu+\xi)\psi(1-\sigma)\beta) \\
C &= [-1+R_0](\mu+\xi)\mathcal{T} \\
\mathcal{T} &= (\mu+\gamma)[(\mu+\omega+\phi)\mu + \omega\phi_-] \\
m &= \frac{\psi(1-\sigma)\beta(\mu+\xi)}{(\mu+\psi(1-\sigma)\phi_-)}(\mu+\xi+\gamma)
\end{aligned}$$

$P(I, R_0)$ has at most two different positive roots. We will show that our model exhibits a backward bifurcation under specific parameter conditions. First, we observe that if $P(I, R_0)$ has real, positive roots, then these roots lie in the interval $(0, 1)$. To justify this claim, we note that $P(I, R_0)$ is a downward-opening quadratic polynomial in I. Additionally, evaluating $P(I, R_0)$ at $I = 1$, we obtain, for all positive R_0,

$$\begin{aligned} P(1, R_0) &= -(1-\sigma)(\mu+\omega)\gamma\psi\beta^2 - (\mu+\omega)(\mu+\psi(1-\sigma)\phi_-)\beta\gamma \\ &\quad -(\mu+\xi)(\mu+\gamma)(\mu+\omega+\phi_+)(1-\sigma)\beta\psi \\ &\quad -(\mu+\gamma)[(\mu+\omega+\phi)\mu+\omega\phi_-](\mu+\xi) \\ &< 0\ . \end{aligned}$$

From the above, it can be stated that, if eq. (5) has positive roots, they must lie within the interval $(0, 1)$. Figure 2 illustrates this statement, for different values of R_0.

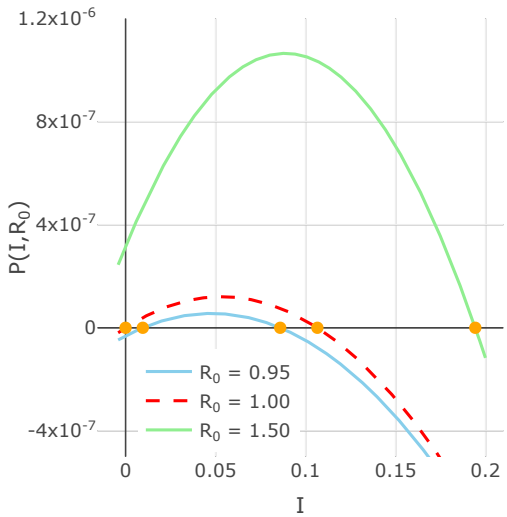

Fig. 2: Graphs of eq. (5) for three values of R_0 as β varies. Here, the polynomial has two positive roots ($R_0 = 0.95$), and one positive root ($R_0 = 1$ and $R_0 = 1.5$). The solid blue, dashed red, and solid green curves correspond to β values of 0.27, 0.2842, and 0.4264, respectively. Orange dots indicate the roots in each case. Other parameter values are $\mu = 0.0000391$, $\omega = 0.02$, $\gamma = 0.0714$, $\xi = 0.0333$, $\sigma = 0.75$, $p = 0.70$, $\psi = 1$ and $T = 35$.

Now, following Islas et al. (2024), we demonstrate that our model exhibits a backward bifurcation under certain parameter conditions. We begin our proof by demonstrating the existence of a positive root in a specific case. Then, we show that there exists a parameter region where two positive roots coexist.

First, we set $R_0 = 1$; then the roots of eq. (5) are

$$I_{01}^* = 0 \quad and \quad I_{02}^* = \frac{(1-D)(\mu+\xi)}{m}.$$

Note that $I_{01}^* = 0$ corresponds to the disease-free equilibrium (P_0). On the other hand, we have that if $1 - D < 0$, then $I_{02}^* \notin (0, 1)$, making it a biologically unfeasible root. However, if the following condition holds,

$$0 < D < 1, \tag{6}$$

it is ensured that $I_{02}^* \in (0, 1)$, and consequently, it is a biologically feasible root. This concludes the case for $R_0 = 1$.

Now, we prove that eq. (5) has two positive roots. First, $P(I, R_0)$ is a continuously differentiable function. Furthermore, we can verify that

$$\frac{\partial P}{\partial I}(I_{01}^*, 1) = (1-D)\mathcal{T} \neq 0, \quad \frac{\partial P}{\partial I}(I_{02}^*, 1) = (D-1)\mathcal{T} \neq 0,$$

when condition (6) holds. Then, by the Implicit Function Theorem (Marsden and Tromba, 2012), there exists a function $g_i(R_0)$, for each of the two equilibrium points indexed by i, such that $P(g_i(R_0), R_0) = 0$ in a neighborhood of $(I_{0i}^*, 1)$. These functions represent the roots of the polynomial, which we denote by $I_i^* = g_i(R_0)$. We express these functions as a series expansion around $R_0 = 1$:

$$I_1^* = g_1(R_0) = \frac{(\mu+\xi)}{(D-1)}(R_0-1) + \mathcal{O}((R_0-1)^2)$$
$$I_2^* = g_2(R_0) = \frac{(1-D)(\mu+\xi)}{m} + \mathcal{O}(R_0-1)$$

Note that for both roots to be positive, it is necessary that the condition (6) holds and that $R_0 < 1$.

Next, we continue the demonstration by determining the range of R_0 for which two positive roots exist. To do this, we calculate the positive root of eq. (5) with multiplicity two, which occurs when the discriminant of eq. (5) is equal to zero. There are two values of R_0 that permit it, which are:

$$R_0^- = \frac{D+2m-\sqrt{4mD[1-D]+4m^2}}{1+4m}, \quad R_0^+ = \frac{D+2m+\sqrt{4mD[1-D]+4m^2}}{1+4m}.$$

From condition (6), we deduce that $0 < 4mD[1-D]+4m^2$. Therefore, R_0^- and R_0^+ are real numbers. Then, when $R_0 = R_0^-$, we obtain

$$I_-^* = \frac{(R_0^- - D)\mathcal{T}}{2\psi(1-\sigma)\beta^2(\mu+\xi+\gamma)(\mu+\omega)},$$

while, when $R_0 = R_0^+$, we have

$$I_+^* = \frac{(R_0^+ - D)\mathcal{T}}{2\psi(1-\sigma)\beta^2(\mu+\xi+\gamma)(\mu+\omega)}.$$

I_-^* and I_+^* are the candidates for the positive root of eq. (5) with multiplicity two. In Appendix B, we prove that $I_-^* < 0$, $0 < I_+^*$, and $0 < R_0^+ < 1$. Therefore, when

$R_0 = R_0^+ < 1$, there is a unique endemic equilibrium given by I_+^*. Consequently, when $R_0^+ < R_0 < 1$, there exist two endemic equilibria.

Finally, to conclude the demonstration, we analyze the scenario when $R_0 > 1$. By Descartes' Rule of Signs, eq. (5) always has a unique positive root. This implies that there is a unique endemic equilibrium.

We summarize our results in the following proposition.

Proposition 3. *Consider Model (3) with D, R_0 and R_0^+ defined above:*

a) A unique endemic equilibrium exists if $R_0 > 1$.

b) If $0 < D < 1$ and $R_0^+ < R_0 < 1$ then there are two endemic equilibria.

c) Otherwise, there is no endemic equilibrium.

4 Numerical simulations.

In this section, we first illustrate the existence of a backward bifurcation (proposition 3) and numerically explore the stability of equilibria when this phenomenon occurs. Then, we examine the impact of the behavioral index, vaccine efficacy, vaccine effectiveness, and other parameters related to vaccine failure on the dynamics of Model (3) and the basic reproduction number, R_0.

4.1 Bi-stability scenario

Figure 3 presents the bifurcation diagram and illustrates the bistability of Model (3) when $R_0^+ < R_0 < 1$. The graph of the backward bifurcation is obtained by varying R_0, which results from varying ψ. This variation is possible because R_0 can also be expressed as a function of ψ (eq. (4)). We use this fact to generate this figure and the subsequent ones that illustrate the backward bifurcation. To achieve this, we assume that behavioral changes modify the behavior before vaccination, ranging from a 95% reduction to an increase of up to three times. That is, ψ varies between 0.05 and 3. Figure 3a shows the bifurcation diagram, where the solid blue line represents stable

equilibrium, and the dashed red line represents unstable equilibrium. Furthermore, it illustrates that the disease-free equilibrium always exists, and if $R_0^+ < R_0 < 1$, there are two endemic equilibria. Figure 3b illustrates a disease dynamics trajectory when the backward bifurcation occurs; we observe a set of initial conditions that lead to a disease-free equilibrium (dashed green lines) and another set that leads to an endemic equilibrium (solid red lines).

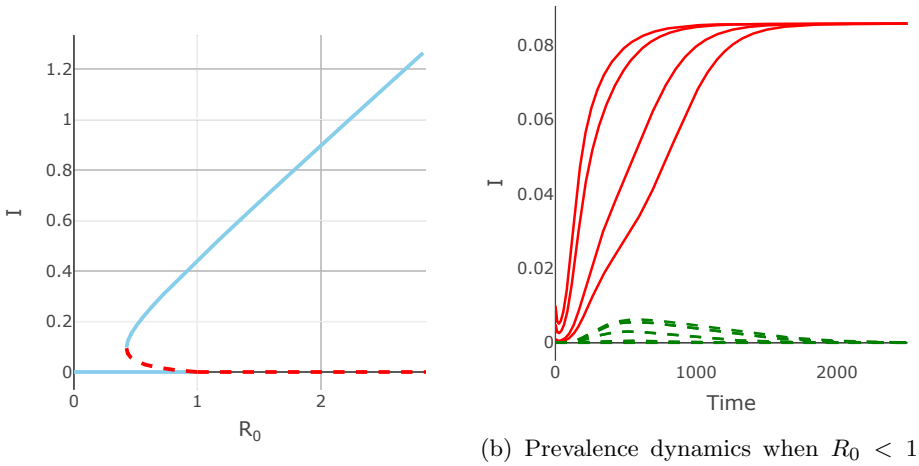

(a) Backward bifurcation for Model (3). The blue and red lines illustrate the stable and unstable equilibria, respectively.

(b) Prevalence dynamics when $R_0 < 1$. Solid red lines illustrate the persistence of the disease. Dashed green lines show the extinction of the disease.

Fig. 3: Dynamics of Model (3) when, except by β and ψ, parameter values are those used in Figure 2. (a) ψ varies between 0.05 and 3. (b) $\psi = 1$. For both cases, $\beta = 0.27$.

4.2 Role of the behavioral index (ψ)

We explore the impact of behavior on backward bifurcations and disease dynamics, using a parametrization for the COVID-19 virus as an example to illustrate these effects.

To this end, we introduce a behavioral index, which models how well non-immune vaccinated individuals follow prevention measures after the vaccine is applied. We categorize this index into three cases:

a) Best case (good) behavior: non-immune vaccinated individuals follow preventive measures strictly, corresponding to values of ψ less than one.

b) Expected (normal) behavior: non-immune vaccinated individuals exhibit the same behavior prior to their vaccination. In this case, the value of ψ equals one.

c) Worst case (bad) behavior: non-immune vaccinated individuals do not comply with the mitigation measures, corresponding to values of ψ greater than one.

These cases allow us to highlight the importance of the behavioral index in Model (3). Figure 4 illustrates the impact of ψ on disease dynamics. Orange, violet, and red lines represent the "good", "normal" and "bad" behavior. In this example, the initial condition is equal to $(S_0, V_{+_0}, V_{-_0}, I_0, R_0) = (0.99, 0, 0, 0.01, 0)$ and, except by ψ, parameter values are those used in Figure 3. We observe that considering a scenario of "good" behavior, the disease will be eradicated, while in other cases, the disease will stabilize at different endemicity levels.

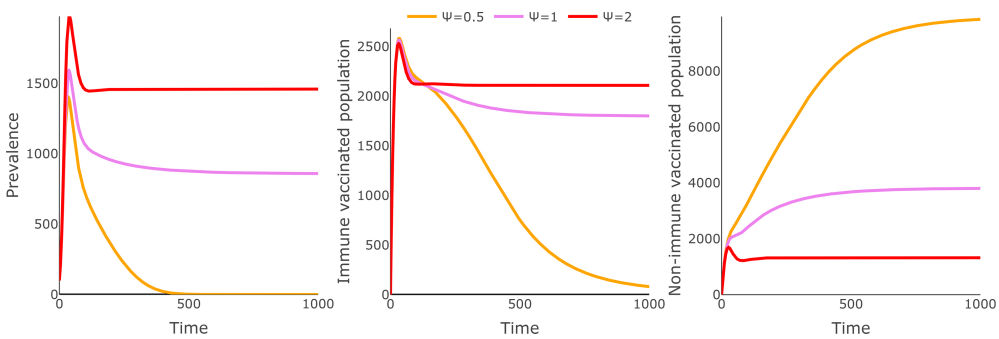

Fig. 4: Cases of behavioral index on disease dynamics. Orange, violet, and red lines represent "good" behavior, "normal" behavior, and "bad" behavior cases, respectively.

4.2.1 Behavioral index threshold (ψ^*)

In the "bad" behavior scenario, the endemic equilibrium is higher than the values in other cases. The question we can now ask is when, ignoring guidelines for mitigation and control, makes it impossible to eradicate the disease. To this end, we introduce an expression for a behavioral index threshold. When the behavioral index exceeds this threshold, the basic reproductive number is always greater than one, indicating that the disease-free equilibrium will be unstable. Consider the scenario where we have an imperfect vaccine ($\sigma \in [0, 1)$), and secondary infections by susceptible people are under control ($R_S < 1$); we define the behavioral index threshold as

$$\psi^* = \frac{\mathcal{T} - \mu\beta(\mu + \omega)}{\beta(\mu + \omega)\phi_-(1 - \sigma)}, \tag{7}$$

where $\mathcal{T} = (\mu + \gamma)[(\mu + \omega + \phi)\mu + \omega\phi_-]$.

Proposition 4. *Let $R_S < 1$. If $\psi > \psi^*$, then $R_0 > 1$*

Proof. Let

$$R_0 = \frac{\beta(\mu + \omega)(\mu + \psi(1 - \sigma)\phi_-)}{\mathcal{T}}$$

By hypothesis, $\psi > \psi^*$ and $R_S < 1$, thus $\psi^* > 0$ is biologically feasible. Then

$$R_0 > \frac{\beta(\mu + \omega)(\mu + \psi^*(1 - \sigma)\phi_-)}{\mathcal{T}}.$$

Substituting the definition of ψ^* in the above inequality, we have

$$\begin{aligned} R_0 &> \frac{\beta(\mu + \omega)\left(\mu + \frac{\mathcal{T} - \mu\beta(\mu+\omega)}{\beta(\mu+\omega)}\right)}{\mathcal{T}} \\ R_0 &> \frac{(\mu\beta(\mu + \omega) + \mathcal{T} - \mu\beta(\mu + \omega))}{\mathcal{T}} = 1. \end{aligned}$$

This completes the proof. □

Figure 5 illustrates Proposition 4, where, except for β, the other parameter values are as in Table 2. Figure 5a shows the relationship between the behavioral index (ψ) and the basic reproductive number (R_0). Here, β is equal to 0.15 and $\psi^* = 1.8387$. The solid blue line illustrates the reproductive number as a function of the behavioral index (ψ) and the red square represents the region where the disease-free equilibrium is stable ($R_0 < 1$). As expected, R_0 increases as ψ increases and, for $\psi > \psi^*$, R_0 is always greater than one. On the other hand, Figure 5b shows the appearance of the backward bifurcation for three different β values. Violet, red and brown curves are obtained when β equals 0.15, 0.20 and 0.25, respectively. For these scenarios, the behavioral index threshold value is equal to 1.8387, 1.348389 and 1.05420, respectively. By the above, we can infer that the behavioral index threshold decreases as the transmission contact rate increases.

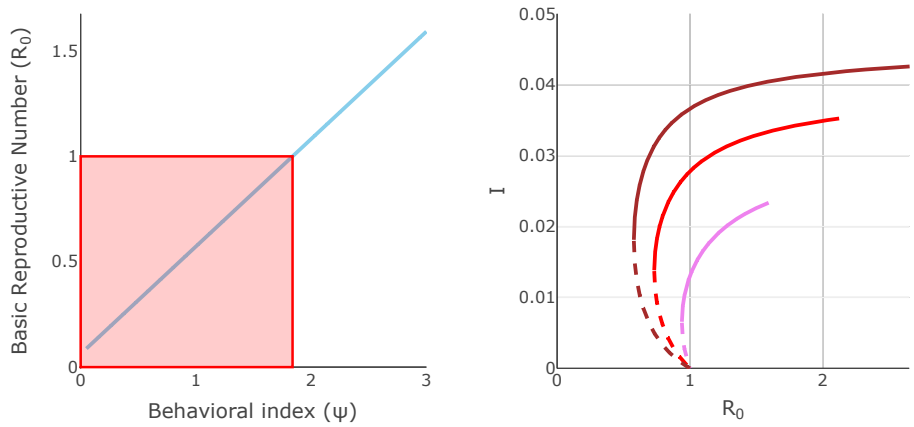

(a) Basic reproductive number as a function of ψ.

(b) Graphs of backward bifurcation for different values of β.

Fig. 5: The behavioral index threshold on backward bifurcation and R_0. (a) The basic reproductive number as function of ψ. The shaded square represents the region. (b) The appearance of the backward bifurcation for three different values of β. Brown, red and violet curves are obtained when $\beta = 0.25$, $\beta = 0.2$ and $\beta = 0.15$, respectively.

Table 2: Parameter values for Model (3) linked to COVID-19 scenario.

Parameter	Value	References
μ	0.00003913	Given[a]
ω	0.005555556	Diaz-Infante et al. (2023)
ξ	0.005555556	Goldberg et al. (2022)
γ	0.07142857	Wölfel et al. (2020)
β	varying	Given[b]
σ	0.746	Emary et al. (2021)
p	0.5	Given[c]
T	180	Given[c]

[a] We assume that the lifespan is 70 years.
[b] The parameter β is solved for in eq. (4), and its value is obtained by fixing R_0 for each observed scenario.
[c] We consider a vaccination campaign with a target coverage of 50% to be achieved in 180 days.

To illustrate the impact of values above or below the behavioral index threshold, we use the COVID-19 parameters as an example (see Table 2). We consider two scenarios: the sub-threshold case, where $1 < \psi < \psi^*$, and the super-threshold case, where $\psi^* \leq \psi$. Figure 6 illustrates these scenarios for the same initial conditions. The solid red line represents the sub-threshold case, specifically $1.5 = \psi < \psi^* = 2.024803$, for which the disease will go extinct. On the other hand, the dashed red line represents the super-threshold case, where $2.024803 = \psi^* < \psi = 2.5$. Here the disease persists.

4.3 The role of σ on R_0

Equation (4) shows the relation between σ and R_0. In fact we have that

$$R_0(1) = \frac{\beta(\mu+\omega)}{(\mu+\gamma)(\mu+\phi+\omega)} < \frac{\beta}{(\mu+\gamma)} = R_0(0) \ .$$

On the other hand, when calculating the basic reproductive number of Model (1), we obtain

$$\hat{R}_0(\sigma) = \frac{\beta(\mu+\omega)}{(\mu+\gamma)(\mu+\omega+\phi)} + \frac{(1-\sigma)\beta\phi}{(\mu+\gamma)(\mu+\omega+\phi)} \ .$$

Obviously, when $\psi = 1$, $\hat{R}_0(0) = R_0(0)$ and $\hat{R}_0(1) = R_0(1)$.

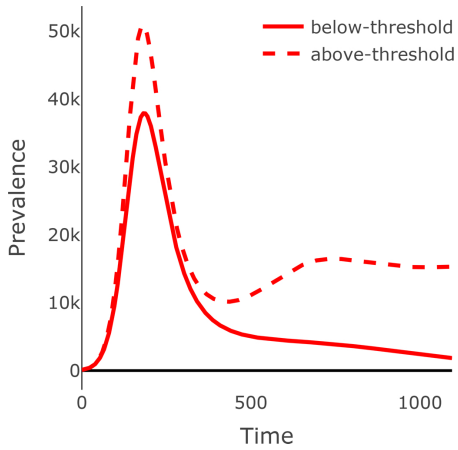

Fig. 6: The impact of the behavioral index threshold on COVID-19 dynamics. For both cases, $\beta = 0.137$, and other parameter values are as given in Table 2. We show two cases: the super-threshold case with $\psi = 1.5$ ($R_0 = 0.7556$), and the subthreshold case with $\psi = 2.5$ ($R_0 = 1.2213$). In this example $\psi^* = 2.024803$.

Figure 7 illustrates the influence of σ on R_0 and the appearance of a backward bifurcation. Figure 7a shows comparison of the reproductive numbers of Model (1) and Model (3) when $\psi = 1$. Here, we observe a threshold value, $\sigma^* > 0$, such that for $\sigma \leq \sigma^*$, the R_0 of Model (3) decreases faster than that of Model (1). However, when $\sigma > \sigma^*$, as σ continues to approach 1, the value of R_0 rises until it matches the R_0 of Model (1). Figure 7b illustrates that, if a backward bifurcation exits, an increase in σ leads to a reduction in the interval length over which bistability is observed. In this figure, solid lines represent stable equilibria, while dashed lines indicate unstable equilibria.

Next, we prove the existence of the threshold $\sigma^* \in (0, 1)$.

Proposition 5. *Let $\phi_+(\sigma)$ and $\phi_-(\sigma)$, and $R_0(\sigma)$ defined as in Section 2 and Equation (4), respectively. Then, there exists $\sigma^* \in (0, 1)$, such that*

$$R_0(\sigma^*) = \min_{\sigma \in (0,1)} R_0(\sigma).$$

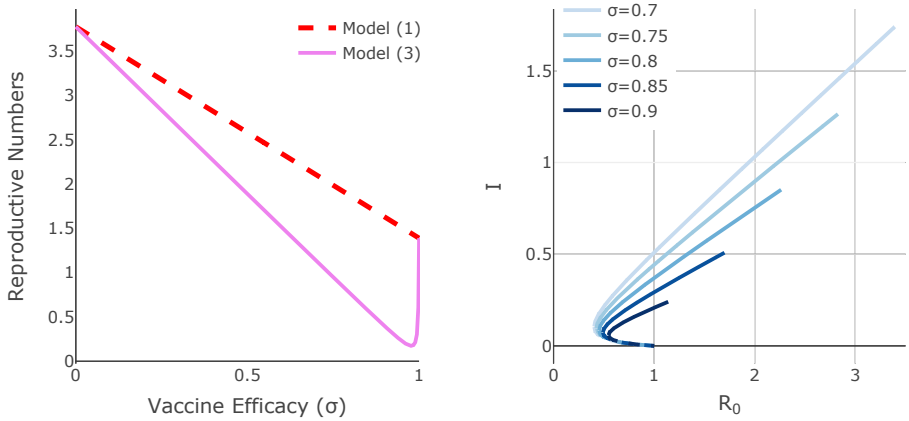

(a) Reproductive number as function of vaccine efficacy for R_0 from Model (3) (solid violet line) and Model (1) (dashed red line).

(b) Backward bifurcation of Model (3) for different values of vaccine efficacy (σ). The intensity of the color thinned as the σ value decreases.

Fig. 7: The impact of vaccine efficacy on reproductive number and backward bifurcation. Except by σ and ψ, other parameters values are similar to used in Figure 3. (a) $\psi = 1$. (b) ψ varies between 0.05 and 3.

Proof. Since

$$\phi_+(\sigma) = -\frac{\ln(1-p\sigma)}{T}, \qquad \phi_-(\sigma) = \frac{1}{T}\ln\left(\frac{1-p\sigma}{1-p}\right) .$$

It is clear that $\phi_+(\sigma), \phi_-(\sigma)$ are continuous functions for all $\sigma \in [0,1]$. Therefore $R_0(\sigma)$ is also a continuous function for all $\sigma \in [0,1]$. Thus, by Weierstrass theorem (Martínez-Legaz, 2014), we can guarantee that exist $\sigma^* \in [0,1]$, such that

$$R_0(\sigma^*) = \min_{\sigma\in[0,1]} R_0(\sigma).$$

We prove now that σ^* is neither 0 nor 1. First, recall that $R_0(1) < R_0(0)$. Thus, $R_0(\sigma)$ does not reach its minimum in $\sigma = 0$. Finally, to guarantee that $R_0(\sigma)$ does not

reach its minimum in $\sigma = 1$, it would be enough to demonstrate that $R_0'(1) > 0$, then

$$R_0'(1) = \frac{\beta(\mu+\omega)\mu p\omega}{(\mu+\gamma)(1-p)\mu^2(\mu+\phi+\omega)^2 T} > 0.$$

□

4.4 Another view of the vaccination rates

McLean and Blower (1993) identify three principal types of vaccine failure: (i) *degree failure*, which may only reduce (without eliminating) the probability of infection upon exposure; (ii) *take failure*, when a vaccine may not affect some people; and (iii) *duration failure*, when a vaccine may confer protection that wanes over time allowing vaccinated individuals to return to the fully susceptible state. In Section 2, we have identified a measure of *vaccine failure* as $1-\sigma$ and we interpret ϕ_- as the vaccination failure rate. We now revisit the idea of MacLean and Blower ($M\&B$) cited above and set:

- $1-\sigma$ as a measure of degree failure,
- $1-\epsilon$ as a measure of take failure, where ϵ is the proportion of vaccinated individual become immune.

We redefine ϕ_+ and ϕ_- as:

$$\phi_+ = \epsilon\phi;\ \phi_- = (1-\epsilon)\phi \tag{8}$$

where $\phi = -\frac{ln(1-p)}{T}$. From now on, in this section, we work with Model (3), but with ϕ_+ and ϕ_- as defined in Equation (8). We refer to this approach as the $M\&B$ Model.

Figure 8 compares results given by Models (1), (3) and M&B. Here, we focus on the reproductive numbers and disease transmission dynamics. To do this, we use the parameter values from Figure 3. Figure 8a shows the $R_0(\sigma)$ behavior for each model when the vaccine efficacy (σ) varies. We observe that the $R_0(\sigma)$ values of the three

models match when $\sigma = 0$. In contrast, when $\sigma = 1$, the $R_0(\sigma)$ values are equal only for Models (1) and (3). On the other hand, for Models (1) and $M\&B$, $R_0(\sigma)$ has a similar behavior for $\sigma \in [0, \sigma^*]$. Figure 8b illustrates the prevalence obtained for each model. We can see that, for sufficiently large time, the prevalence given by Model (1) is higher than that of Model (3) and the $M\&B$ Model, and their prevalences are very similar throughout the simulation time.

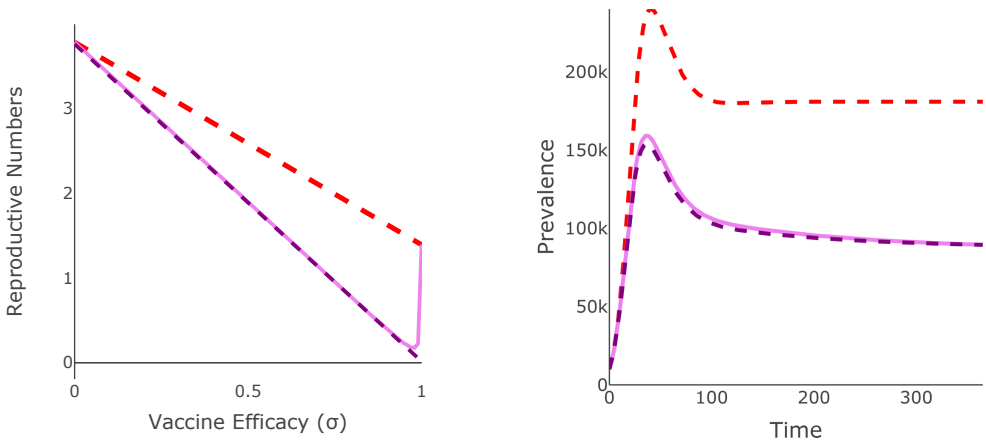

(a) Vaccine efficacy over R_0 for each cases.

(b) The prevalence for each case.

Fig. 8: The role of vaccine efficacy over the reproductive number and disease dynamics. Red dashed lines illustrate the results of Model (1). Violet solid lines show the results of Model (3). Purple dashed lines illustrate the results of M&B Model. Here, $\epsilon = 0.75$, and except for σ, the other parameter values are the same as those used in Figure 3b. (a) σ varies between 0 and 1. (b) $\sigma = 0.75$.

4.5 Vaccine effectiveness

Vaccine effectiveness (V_{Eff}) is determined by comparing infection rates between vaccinated and unvaccinated individuals (Bodner et al., 2023). This indicator helps to evaluate how well a vaccine protects a population under uncontrolled conditions. In this section, we proceed to calculate this indicator. To do this, we follow Haber (1999)

and Bodner et al. (2023). Specifically, we define

$$V_{Eff}(t) = 1 - RR(t),$$

where $RR(t)$ is the relative risk at time t, defined as

$$RR(t) = \frac{\frac{CI_v(t)}{N_v}}{\frac{CI_u(t)}{N_u}}.$$

Data used to calculate $V_{Eff}(t)$ are obtained from the solution of Model (3), assuming that non-immune but vaccinated individuals (V_-) either maintain or worsen their behavior after vaccination ($\psi \geq 1$). We consider N_v as the total population of vaccinated individuals, $N_v = V_+ + V_-$. We model N_u as $S + (1-p)(I+R)$ where p represents the vaccine coverage. We propose this approximation to account for vaccinated and unvaccinated individuals in the infected and recovered classes of Model (3).

Now, we explore the dynamics of vaccine effectiveness through three scenarios. Except for the parameter values specified in each scenario, all others are given in Table 2.

- **Scenario 1: Impact of the initial number of infected individuals.** We consider the initial prevalence $I(0)$ to be 0.01%, 0.0001% and 0.000001% of a total population of 10^8 people as the initial percentage of infected individuals. The initial values of all other compartments, except by susceptible class, are set to zero. Here, we explore the scenario where $R_0 = 3.7826$. Thus, we set $\beta = 0.137$.
- **Scenario 2: Effect of increasing the behavioral index value.** This scenario examines the impact of increasing the value of ψ. We take ψ to be equal to 4, 8 and 12, while setting $\beta = 0.137$.
- **Scenario 3: Role of the basic reproductive number.** This scenario explores the impact of varying β and ψ while keeping R_0 around a fixed value. In one case,

we set $\beta = 1.049$ and $\psi = 1$, while in the other case, $\beta = 0.145$ and $\psi = 8$. In both cases, R_0 is close to 4.003.

Figure 9 illustrates Scenario 1 when $\psi = 8$. For this scenario, regardless of the initial conditions, the disease exhibits persistence. However, depending on the initial condition, the vaccine effectiveness can take negative values during a period of time. This scenario also illustrates that only varying the initial condition, the appearance of negative values in vaccine effectiveness is related to the growth rate of the epidemic curve.

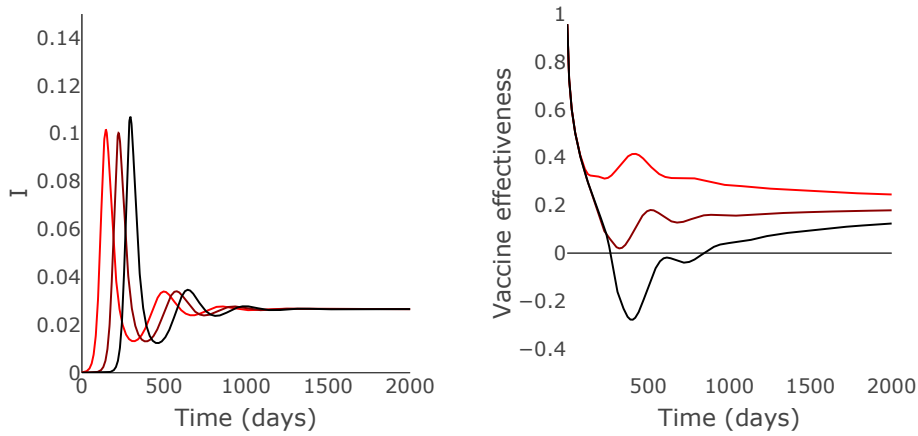

Fig. 9: Scenario 1: Impact of the initial number of infected individuals. The red, brown, and black solid lines is obtained when the initial percentage of infected individuals is 0.01%, 0.0001% and 0.000001%, respectively.

Figure 10 shows the results of Scenario 2 when considering the second initial percentage of infected individuals from Scenario 1, specifically 0.0001%. In contrast to Scenario 1, we observe that for these parameter combinations, there exists a value of ψ that makes V_{Eff} negative for a period of time. This occurs as a consequence of the increase in the behavioral index, which accelerates the growth of the epidemic outbreak.

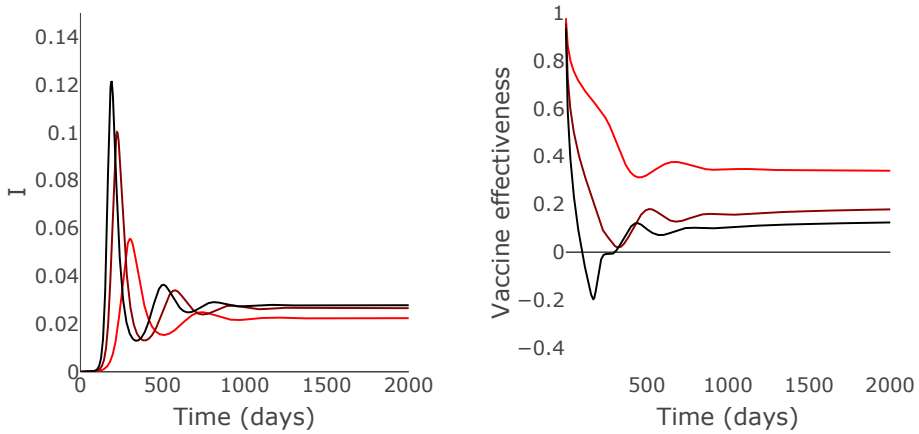

Fig. 10: Scenario 2: Effect of increasing the behavioral index value. The red, brown, and black solid lines represent dynamics when ψ value is equal to 4, 8 and 12, respectively.

Scenario 3 is illustrated in Figure 11, considering the smallest initial percentage of infected individuals from Scenario 1, 0.000001%. We explore the impact of similar values of R_0 when considering (i) a high transmission rate and a low behavioral index and (ii) a high ψ and a low β. Recall that ψ only affects non-immune vaccinated, so an increase in ψ will impact CI_v but not CI_u. Figure 11 shows that similar values of R_0 can lead to notable changes in vaccine effectiveness. We observe that variations in vaccine effectiveness may depend more on the behavioral index than on transmission rates.

5 Conclusions

Motivated by the absence of complete immunity of vaccines for respiratory diseases (Safan and Rihan, 2014), our work explores the impact of the behavioral change of non-immune vaccinated individuals on disease transmission dynamics and other indexes, such as the basic reproductive number and vaccine effectiveness.

Our results prove that the disease can persist even when the basic reproductive number (R_0) is less than one. This suggests that our model exhibits a backward

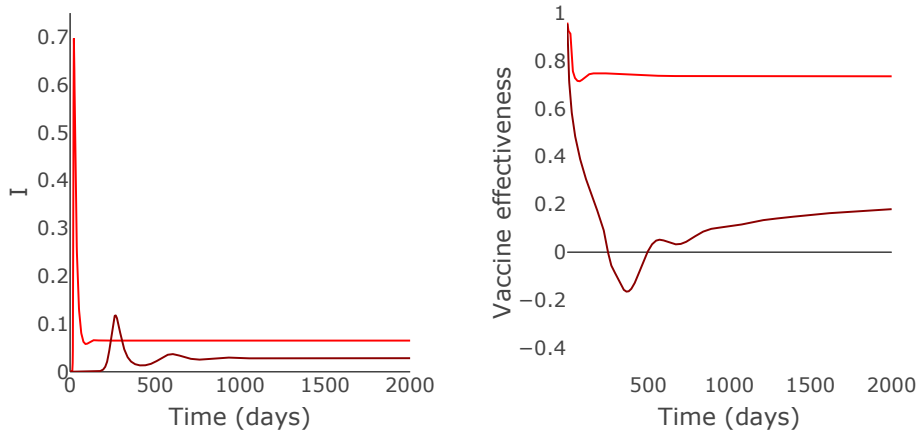

Fig. 11: Scenario 3: Role of the basic reproductive number. The red and brown solid lines illustrate the cases when $(\beta = 1.049, \psi = 1)$ and $(\beta = 0.145, \psi = 8)$, respectively. For both cases, the R_0 value is close to 4.003.

bifurcation. This finding aligns with previous models that include a single vaccinated compartment (Kribs-Zaleta and Velasco-Hernández, 2000; Arino et al., 2003). On the other hand, we observe that R_0 linearly depends on ψ, which allows us to find a threshold value of the behavioral index (ψ^*). This threshold ensures that for any ψ greater than ψ^*, the value of R_0 is always greater than one. We also observe that ψ^* decreases as the transmission contact rate increases. This implies that when the transmission contact rate is high, reducing the behavioral change of the non-immune vaccinated population would not be sufficient to eradicate the disease.

As previously mentioned, the behavioral index impacts both R_0 and backward bifurcation. Figure 4 shows that disease eradication becomes possible when non-immune vaccinated individuals strictly follow preventive measures. In contrast, the disease will always persist if non-immune vaccinated individuals do not comply with preventive measures and the values of ψ exceed ψ^*. This reinforces the importance of maintaining preventive measures even after vaccine application.

Bodner et al. (2023) reported that during the presence of the Omicron variant in the COVID-19 pandemic, observational studies suggested negative vaccine effectiveness. In their study, the authors observed that vaccinated-contact heterogeneity could feasibly lead to negative measurements of vaccine effectiveness. Motivated by these findings, we used our model to explore vaccine effectiveness. Our numerical results highlight the role of the behavioral index in vaccine effectiveness. Figures 10 and 11 show that ψ has a more significant impact on vaccine effectiveness than β in producing negative vaccine effectiveness. This is consistent with the findings in Bodner et al. (2023), as we model the behavioral index as a perturbation of the transmission contact rate of non-immune vaccinated individuals, introducing contact heterogeneity within the vaccinated population. However, we also observed that the initial number of infected individuals could contribute to negative vaccine effectiveness, which, to our knowledge, has not been previously reported. Finally, our simulations illustrate that this phenomenon occurred during epidemic growth, which is also consistent with the findings reported by Bodner et al. (2023).

It is important to mention that, we have only considered the behavioral change of non-immune vaccinated individuals and, like other studies, assumed homogeneity in the population. However, we believe incorporating behavioral changes in other classes, splitting the population by age structure or social determinants such as poverty levels, and including vaccination schedules are crucial for providing more specific and realistic scenarios. We will address these limitations in future work.

Acknowledgments

We acknowledge support from the Joint Cooperation Fund Chile-Mexico 2022: Mathematical Modeling of Epidemic Processes, Incorporating Population Structure, Regional Distribution and Risk Groups. We also thank Luca Ferretti and Jonathan Dushoff for their insightful comments on a previous version of this work.

Declarations

This work has not been published or considered for publication elsewhere. We have no conflicts of interest to disclose. We also confirm that all co-authors have agreed to the present submitted version.

References

Arino, J., Cooke, K., Van Den Driessche, P., Velasco-Hernández, J.: An epidemiology model that includes a leaky vaccine with a general waning function. Discrete and Continuous Dynamical Systems Series B **4**(2), 479–495 (2004) https://doi.org/10.3934/dcdsb.2004.4.479

Arino, J., McCluskey, C.C., Driessche, P.: Global results for an epidemic model with vaccination that exhibits backward bifurcation. SIAM Journal on Applied Mathematics **64**(1), 260–276 (2003) https://doi.org/10.1137/S003613990241382

Allen, L.J., Driessche, P.: Stochastic epidemic models with a backward bifurcation. Mathematical Biosciences & Engineering **3**(3), 445–458 (2006) https://doi.org/10.3934/mbe.2006.3.445

Acuña-Zegarra, M.A., Díaz-Infante, S., Baca-Carrasco, D., Olmos-Liceaga, D.: COVID-19 optimal vaccination policies: A modeling study on efficacy, natural and vaccine-induced immunity responses. Mathematical Biosciences **337**, 108614 (2021) https://doi.org/10.1016/j.mbs.2021.108614

Acuña-Zegarra, M.A., Santana-Cibrian, M., Velasco-Hernandez, J.X.: Modeling behavioral change and COVID-19 containment in Mexico: A trade-off between lockdown and compliance. Mathematical biosciences **325**, 108370 (2020) https://doi.org/10.1016/j.mbs.2020.108370

Bodner, K., Knight, J., Hamilton, M.A., Mishra, S.: Testing whether higher contact among the vaccinated can be a mechanism for observed negative vaccine effectiveness. American Journal of Epidemiology **192**(8), 1335–1340 (2023) https://doi.org/10.1093/aje/kwad055

Colmegna, I., Valerio, V., Amiable, N., Useche, M., Rampakakis, E., Flamand, L., Rollet-Labelle, E., Bessette, L., Fitzcharles, M.-A., Hazel, E., *et al.*: COVID-19 Vaccine in Immunosuppressed Adults with Autoimmune rheumatic Diseases (COVIAAD): safety, immunogenicity and antibody persistence at 12 months following Moderna Spikevax primary series. RMD open **9**(4), 003400 (2023) https://doi.org/10.1136/rmdopen-2023-003400

Diaz Granados, C.A., Dunning, A.J., Kimmel, M., Kirby, D., Treanor, J., Collins, A., Pollak, R., Christoff, J., Earl, J., Landolfi, V., *et al.*: Efficacy of high-dose versus standard-dose influenza vaccine in older adults. New England Journal of Medicine **371**(7), 635–645 (2014) https://doi.org/10.1056/NEJMoa1315727

Dushoff, J., Huang, W., Castillo-Chavez, C.: Backwards bifurcations and catastrophe in simple models of fatal diseases. Journal of mathematical biology **36**, 227–248 (1998) https://doi.org/10.1007/s002850050099

Diaz-Infante, S., Acuña-Zegarra, M.A., Velasco-Hernández, J.X.: Modeling a traffic light warning system for acute respiratory infections. Applied Mathematical Modelling **121**, 217–230 (2023) https://doi.org/10.1016/j.apm.2023.04.029

Emary, K.R., Golubchik, T., Aley, P.K., Ariani, C.V., Angus, B., Bibi, S., Blane, B., Bonsall, D., Cicconi, P., Charlton, S., *et al.*: Efficacy of chadox1 ncov-19 (azd1222) vaccine against sars-cov-2 variant of concern 202012/01 (b. 1.1. 7): an exploratory analysis of a randomised controlled trial. The Lancet **397**(10282), 1351–1362 (2021) https://doi.org/10.1016/S0140-6736(21)00628-0

Gemmetto, V., Barrat, A., Cattuto, C.: Mitigation of infectious disease at school: targeted class closure vs school closure. BMC infectious diseases **14**, 1–10 (2014) https://doi.org/10.1186/s12879-014-0695-9

Greenhalgh, D., Doyle, M., Lewis, F.: A mathematical treatment of AIDS and condom use. Mathematical Medicine and Biology: A Journal of the IMA **18**(3), 225–262 (2001) https://doi.org/10.1093/imammb/18.3.225

Goldberg, Y., Mandel, M., Bar-On, Y.M., Bodenheimer, O., Freedman, L.S., Ash, N., Alroy-Preis, S., Huppert, A., Milo, R.: Protection and waning of natural and hybrid immunity to SARS-CoV-2. New England Journal of Medicine **386**(23), 2201–2212 (2022) https://doi.org/10.1056/NEJMoa2118946

Gumel, A.B.: Causes of backward bifurcations in some epidemiological models. Journal of Mathematical Analysis and Applications **395**(1), 355–365 (2012) https://doi.org/10.1016/j.jmaa.2012.04.077

Ghiasi, N., Valizadeh, R., Arabsorkhi, M., Hoseyni, T.S., Esfandiari, K., Sadighpour, T., Jahantigh, H.R.: Efficacy and side effects of Sputnik V, Sinopharm and AstraZeneca vaccines to stop COVID-19; a review and discussion. Immunopathologia Persa **7**(2), 31 (2021) https://doi.org/10.34172/ipp.2021.31

Haber, M.: Estimation of the direct and indirect effects of vaccination. Statistics in medicine **18**(16), 2101–2109 (1999) https://doi.org/10.1002/(SICI)1097-0258(19990830)18:16⟨2101::AID-SIM178⟩3.0.CO;2-6

Hadeler, K.P., Castillo-Chávez, C.: A core group model for disease transmission. Mathematical biosciences **128**(1-2), 41–55 (1995) https://doi.org/10.1016/0025-5564(94)00066-9

Halloran, M.E., Haber, M., Longini Jr, I.M.: Interpretation and estimation of vaccine

efficacy under heterogeneity. American Journal of Epidemiology **136**(3), 328–343 (1992) https://doi.org/10.1093/oxfordjournals.aje.a116498

Halloran, M.E., Haber, M., Longini Jr, I.M., Struchiner, C.J.: Direct and indirect effects in vaccine efficacy and effectiveness. American journal of epidemiology **133**(4), 323–331 (1991) https://doi.org/10.1093/oxfordjournals.aje.a115884

Hu, Z., Ma, W., Ruan, S.: Analysis of sir epidemic models with nonlinear incidence rate and treatment. Mathematical biosciences **238**(1), 12–20 (2012)

Hsieh, Y.-H.: Age groups and spread of influenza: implications for vaccination strategy. BMC infectious diseases **10**, 1–12 (2010) https://doi.org/10.1186/1471-2334-10-106

Hsieh, Y.-H., Velasco-Hernandez, J.X.: Community treatment of hiv-1: initial stage and asymptotic dynamics. Biosystems **35**(1), 75–81 (1995) https://doi.org/10.1016/0303-2647(94)01482-M

Islas, J.M., Corona-Moreno, R., Velasco-Hernández, J.X.: Multiple endemic equilibria in an environmentally-transmitted disease with three disease stages. Mathematical Biosciences **375**, 109244 (2024) https://doi.org/10.1016/j.mbs.2024.109244

Kar, T.K., Mondal, P.K.: Global dynamics of a tuberculosis epidemic model and the influence of backward bifurcation. Journal of Mathematical Modelling and Algorithms **11**, 433–459 (2012) https://doi.org/10.1007/s10852-012-9210-8

Kribs-Zaleta, C.M., Martcheva, M.: Vaccination strategies and backward bifurcation in an age-since-infection structured model. Mathematical biosciences **177**, 317–332 (2002) https://doi.org/10.1016/S0025-5564(01)00099-2

Kribs-Zaleta, C.M., Velasco-Hernández, J.X.: A simple vaccination model with multiple endemic states. Mathematical biosciences **164**(2), 183–201 (2000) https://doi.

org/10.1016/S0025-5564(00)00003-1

McLean, A.R., Blower, S.M.: Imperfect vaccines and herd immunity to HIV. Proceedings of the Royal Society of London. Series B: Biological Sciences **253**(1336), 9–13 (1993) https://doi.org/10.1098/rspb.1993.0075

Martínez-Legaz, J.E.: On weierstrass extreme value theorem. Optimization letters **8**(1), 391–393 (2014) https://doi.org/10.1007/s11590-012-0587-0

Magpantay, F.M.G., Riolo, M.A., Cellès, M.D., King, A.A., Rohani, P.: Epidemiological consequences of imperfect vaccines for immunizing infections. SIAM Journal on Applied Mathematics **74**(6), 1810–1830 (2014) https://doi.org/10.1137/140956695

Marsden, J.E., Tromba, A.J.: Vector Calculus, 6th edn. W. H. Freeman and Company, New York (2012)

Ray, R., Dos Santos, G., Buck, P.O., Claeys, C., Matias, G., Innis, B.L., Bekkat-Berkani, R.: A review of the value of quadrivalent influenza vaccines and their potential contribution to influenza control. Human vaccines & immunotherapeutics **13**(7), 1640–1652 (2017) https://doi.org/10.1080/21645515.2017.1313375

Seale, H., Dyer, C.E., Abdi, I., Rahman, K.M., Sun, Y., Qureshi, M.O., Dowell-Day, A., Sward, J., Islam, M.S.: Improving the impact of non-pharmaceutical interventions during COVID-19: examining the factors that influence engagement and the impact on individuals. BMC Infectious Diseases **20**, 1–13 (2020) https://doi.org/10.1186/s12879-020-05340-9

Sadoff, J., Gray, G., Vandebosch, A., Cárdenas, V., Shukarev, G., Grinsztejn, B., Goepfert, P.A., Truyers, C., Van Dromme, I., Spiessens, B., *et al.*: Final analysis of efficacy and safety of single-dose Ad26. COV2. S. New England Journal of Medicine **386**(9), 847–860 (2022) https://doi.org/10.1056/NEJMoa2117608

Safan, M., Rihan, F.A.: Mathematical analysis of an SIS model with imperfect vaccination and backward bifurcation. Mathematics and Computers in Simulation **96**, 195–206 (2014) https://doi.org/10.1016/j.matcom.2011.07.007

Smith, P.G., Rodrigues, L.C., Fine, P.: Assessment of the protective efficacy of vaccines against common diseases using case-control and cohort studies. International journal of epidemiology **13**(1), 87–93 (1984) https://doi.org/10.1093/ije/13.1.87

Saldaña, F., Velasco-Hernández, J.X.: The trade-off between mobility and vaccination for COVID-19 control: A metapopulation modelling approach. Royal Society Open Science **8**(6), 202240 (2021) https://doi.org/10.1098/rsos.202240

Saldaña, F., Velasco-Hernández, J.X.: Modeling the COVID-19 pandemic: a primer and overview of mathematical epidemiology. SeMA Journal **79**(2), 225–251 (2022) https://doi.org/10.1007/s40324-021-00260-3

Velasco-Hernández, J.X., , M., Comas-García, A., Cherpitel, D.E.N., Ocampo, M.C.: Superinfection between influenza and rsv alternating patterns in san luis potosí state, méxico. PLOS ONE **10**(3), 1–19 (2015) https://doi.org/10.1371/journal.pone.0115674

Van den Driessche, P., Watmough, J.: Reproduction numbers and sub-threshold endemic equilibria for compartmental models of disease transmission. Mathematical Biosciences **180**(1), 29–48 (2002) https://doi.org/10.1016/S0025-5564(02)00108-6

Wölfel, R., Corman, V.M., Guggemos, W., Seilmaier, M., Zange, S., Müller, M.A., Niemeyer, D., Jones, T.C., Vollmar, P., Rothe, C., *et al.*: Virological assessment of hospitalized patients with COVID-2019. Nature **581**(7809), 465–469 (2020) https://doi.org/10.1038/s41586-020-2196-x

World Health Organization: Vaccine efficacy, effectiveness and protection (2021). https://www.who.int/news-room/feature-stories/detail/vaccine-efficacy-effectiveness-and-protection Accessed 28-01-2025

Wu, Q., Tong, J., Zhang, B., Zhang, D., Chen, J., Lei, Y., Lu, Y., Wang, Y., Li, L., Shen, Y., *et al.*: Real-world effectiveness of BNT162b2 against infection and severe diseases in children and adolescents. Annals of Internal Medicine **177**(2), 165–176 (2024) https://doi.org/10.7326/M23-1754

Xue, L., Ren, X., Magpantay, F., Sun, W., Zhu, H.: Optimal control of mitigation strategies for dengue virus transmission. Bulletin of Mathematical Biology **83**, 1–28 (2021) https://doi.org/10.1007/s11538-020-00839-3

Appendix A Invariance and positive region

Proposition 1. Let $\Omega = \{(V_+, V_-, I, R) | 0 \leq V_+, 0 \leq V_-, 0 \leq I, 0 \leq R, V_+ + V_- + I + R \leq 1\}$. Then Ω is a positively invariant set under the flow of Model (3).

Proof. From Model (3), we analyze the vector field on the hyperplanes where each variable is set to zero.

$$\begin{aligned}
\frac{\partial V_+}{\partial t} |_{V_+=0} &= \phi_+(1 - V_- - I - R) > 0 \\
\frac{\partial V_-}{\partial t} |_{V_-=0} &= \phi_+(1 - V_+ - I - R) > 0 \\
\frac{\partial I}{\partial t} |_{I=0} &= 0 \\
\frac{\partial R}{\partial t} |_{R=0} &= \gamma I > 0
\end{aligned}$$

By the above, we guarantee that for an initial condition in the positive orthant, the solution remains in the positive orthant. Finally, we will prove that for any initial condition in the hyperplane $V_+ + V_- + I + R = 1$, the solutions of Model (3) remain

in Ω. Let $V_+^0, V_-^0, I^0, R^0 > 0$, such that $V_+^0 + V_-^0 + I^0 + R^0 = 1$, then

$$\begin{aligned}
(1,1,1,1)\cdot(\dot{V}_+, \dot{V}_-, \dot{I}, \dot{R})\,|_{(V_+^0, V_-^0, I^0, R^0)} &= \dot{V}_+ + \dot{V}_- + \dot{I} + \dot{R}\,|_{(V_+^0, V_-^0, I^0, R^0)} \\
&= (\phi + \beta I)(1 - V_+^0 - V_-^0 - I^0 - R^0) \\
&\quad -\mu(V_+^0 + V_-^0 + I^0 + R^0) - \omega V_+^0 - \xi R^0 \\
&= -\mu(V_+^0 + V_-^0 + I^0 + R^0) - \omega V_+^0 - \xi R^0
\end{aligned}$$

The above allows us to conclude that for any initial condition in Ω, its solution will remain in Ω. □

Appendix B Backward bifurcation

In this section, we prove that the vertex of the parabola associated with the backward bifurcation is (R_0^+, I_+^*).

Proof. We first prove that $I_-^* < 0$. Note that, to establish this, it is sufficient to show that $R_0^- - D < 0$, thus

$$\begin{aligned}
R_0^- - D &= \frac{D + 2m - \sqrt{4mD[1-D] + 4m^2}}{1+4m} - D \\
&= \frac{D + 2m - \sqrt{4mD[1-D] + 4m^2} - D(1+4m)}{1+4m} \\
&= \frac{2m(1-2D) - \sqrt{4mD[1-D] + 4m^2}}{1+4m} \\
&\leq \frac{2m(1-2D) - \sqrt{4m^2}}{1+4m} \\
&\leq \frac{-4mD}{1+4m} \\
&< 0 \qquad \text{(by condition (6))}
\end{aligned}$$

Therefore, $I_-^* < 0$. Consequently, (R_0^-, I_-^*) is not the vertex of the parabola associated with the backward bifurcation.

Now, we demonstrate that $0 < R_0^+ < 1$. The proof that $0 < R_0^+$ is immediately. On the other hand,

$$
\begin{aligned}
R_0^+ < 1 &\Leftrightarrow D + 2m + \sqrt{4mD[1-D] + 4m^2} < 1 + 4m \\
&\Leftrightarrow 4mD[1-D] + 4m^2 < ((1-D) + 2m)^2 \\
&\Leftrightarrow 4mD[1-D] + 4m^2 < (1-D)^2 + 4m(1-D) + 4m^2 \\
&\Leftrightarrow 4mD[1-D] < (1-D)^2 + 4m(1-D) \\
&\Leftrightarrow 0 < (1-D)((1-D) + 4m - 4mD) \\
&\Leftrightarrow 0 < (1-D)((1-D) + 4m(1-D)) \\
&\Leftrightarrow 0 < (1-D)^2(1+4m)
\end{aligned}
$$

Thus, we guarantee that $0 < R_0^+ < 1$. To conclude the proof, we demonstrate that $I_+^* \in (0,1)$. We begin by proving that $0 < I_+^*$, for which it is sufficient to show that $R_0^+ - D > 0$. Then

$$
\begin{aligned}
R_0^+ - D &= \frac{D + 2m + \sqrt{4mD[1-D] + 4m^2}}{1+4m} - D \\
&= \frac{D + 2m - D(1+4m) + \sqrt{4mD[1-D] + 4m^2}}{1+4m} \\
&= \frac{2m - 4mD + \sqrt{4mD[1-D] + 4m^2}}{1+4m} \\
&\geq \frac{2m - 4mD + \sqrt{4m^2}}{1+4m} \\
&\geq \frac{4m - 4mD}{1+4m} \\
&\geq \frac{4m(1-D)}{1+4m} \\
&> 0 \qquad \text{(by condition (6))}
\end{aligned}
$$

Therefore, we conclude that $0 < I_+^*$. Finally, as we proved at the beginning of Section 3.2, if the root of eq. (5) is positive, then it must be less than one. Hence,

$0 < I_+^* < 1$. Consequently, the vertex of the parabola associated with the backward bifurcation is (R_0^+, I_+^*).

$\square$